Conf-931117--2

PNL-SA-23289

ANALYSIS OF MID-TROPOSPHERIC CARBON MONOXIDE DATA USING A THREE-DIMENSIONAL GLOBAL ATMOSPHERIC CHEMISTRY NUMERICAL MODEL

R. C. Easter
R. D. Saylor
E. G. Chapman

November - December 1993

Presented at the
20th International Technical Meeting on
Air Pollution Modelling and its Application
November 29 - December 3, 1993
Valencia, Spain

Work supported by
the U.S. Department of Energy
under Contract DE-AC06-76RLO 1830

Pacific Northwest Laboratory
Richland, Washington 99352

DISCLAIMER

This report was prepared as an account of work sponsored by an agency of the United States Government. Neither the United States Government nor any agency thereof, nor any of their employees, makes any warranty, express or implied, or assumes any legal liability or responsibility for the accuracy, completeness, or usefulness of any information, apparatus, product, or process disclosed, or represents that its use would not infringe privately owned rights. Reference herein to any specific commercial product, process, or service by trade name, trademark, manufacturer, or otherwise does not necessarily constitute or imply its endorsement, recommendation, or favoring by the United States Government or any agency thereof. The views and opinions of authors expressed herein do not necessarily state or reflect those of the United States Government or any agency thereof.

MASTER

DISTRIBUTION OF THIS DOCUMENT IS UNLIMITED

ANALYSIS OF MID-TROPOSPHERIC CARBON MONOXIDE DATA USING A THREE-DIMENSIONAL GLOBAL ATMOSPHERIC CHEMISTRY NUMERICAL MODEL

Richard C. Easter, Rick D. Saylor, and Elaine G. Chapman

Earth and Environmental Sciences Center
Pacific Northwest Laboratory
Richland, WA 99352

INTRODUCTION

Carbon monoxide is an important atmospheric trace species. It has long been recognized as a major contributor to urban air quality and in high concentrations is known to adversely affect health (Seinfeld, 1986). CO is the third most abundant carbon-containing species in the atmosphere and its reaction with hydroxyl radical (OH) represents a 2000-3000 Tg/yr (1 Tg = 10^{12} g) source of carbon dioxide. On a global basis, CO is the dominant sink for OH (Logan *et al.*, 1981) and therefore plays a significant role in the troposphere's overall oxidative capacity. Furthermore, depending on the local abundance of nitrogen oxides, CO can participate in reactions that either increase or decrease the formation of tropospheric ozone (Logan *et al.*, 1981).

Several three-dimensional modeling studies have been attempted in the past to better understand the global distribution of CO. The earliest attempt was made by Kwok *et al.* (1971). In their simulation, CO was transported within a GCM as an inert tracer and allowed to advect within the troposphere over 30 days during a simulated November-December time period. They performed experiments with and without vertical CO transport by cumulus convection and found that around 10 percent of their model's global-mean vertical transport occurred through upward cumulus motion. Peters and Jouvanis (1979) developed a global CO and CH_4 transport model that included chemical kinetics calculations and was separated from a parent GCM such that observed meteorological data for a specified time period could be used to drive a simulation. From their simulations they estimated a residence time for CO of 0.21 yr. The same model was used by Kitada and Peters (1982) to generate global estimates of the distribution of OH concentrations which compared favorably with the limited measurements available at that time. Pinto *et al.* (1983) used a GCM tracer model with simple chemistry to study the climatological CO budget and its global distribution. They suggested that, in addition to fossil fuel combustion and CH_4 oxidation sources of CO, a large low latitude source of 1300 Tg/yr was necessary to account for observed CO magnitudes and isotopic abundances. Crutzen and Zimmerman (1991) performed a set of global three-dimensional simulations to study the impact of changing anthropogenic emissions of CO, CH_4, and NO_x from pre-industrial values to present-day levels on the atmosphere's total oxidative capacity. They concluded that since the beginning of the industrial revolution a large increase in CO concentrations has occurred, predominantly in the northern hemisphere, which has resulted in a substantial decrease of global OH concentrations. In Saylor and Peters (1990, 1991), the original model of Peters and Jouvanis (1979) was used to analyze CO data from the November 1981 mission of NASA's Measurement of Air Pollution from Satellites (MAPS) program. A three-dimensional simulation was performed for the November 1981 time period and the model's results were compared with the mid- to upper-tropospheric data of Reichle *et al.* (1986). They found good agreement between the model's results and the observations of the MAPS experiment. Simulations performed without the inclusion of fossil fuel combustion emissions indicated that emissions from biomass burning may be exerting a significant role in global CO distributions.

The purpose of the current work is to extend the results of Saylor and Peters (1990, 1991) to the October 1984 MAPS CO dataset. The data obtained during the second MAPS mission was much more complete in global coverage and thus provides an excellent opportunity for comparison with model simulations. The primary objective of this study is to examine the data of the 1984 MAPS mission, using a three-dimensional model as an interpretive tool. We have performed global, three-dimensional simulations of CO transport and chemistry for September-October, 1984, the time period during which the MAPS experiment was conducted.

MAPS MEASUREMENTS OF TROPOSPHERIC CARBON MONOXIDE

The Measurement of Air Pollution from Satellites (MAPS) experiment was designed by NASA to investigate the global distribution of tropospheric CO (Reichle *et al.*, 1986; Reichle *et al.*, 1990). Two experiments have been conducted in this program - the first during November 1981 and the second during October 1984. In each experiment a nadir-viewing gas filter radiometer was placed onboard the U.S. space shuttle and mid- to upper-tropospheric CO data were obtained. Details of the measurement technique and instrumentation used during these experiments can be found in Reichle *et al.* (1986, 1990). Carbon monoxide measurements were made between 38° N and 38° S during the 1981 experiment, while a broader coverage of 57° N to 57° S was obtained during the 1984 experiment. The MAPS measurements represent the first nearly simultaneous set of trace tropospheric species data obtained with such widespread global coverage. In this work we concentrate our analysis on the second MAPS experiment, although some of the major features of the 1984 dataset are also common to the 1981 data.

The second MAPS experiment was performed during October 5-13, 1984; Reichle *et al.* (1990) present results from this dataset. In comparing remotely sensed CO mixing ratios from the MAPS experiment with *in situ* CO measurements taken in the mid-troposphere by aircraft sampling, Reichle et al. (1990) concluded that the MAPS CO data are systematically too low by 20-40 percent. Taking this bias into account, several large-scale features of the MAPS dataset are described in the following. Significant areas of elevated CO mixing ratios (> 80 ppb) occur over southern Africa, central South America and central and eastern Asia. Smaller areas of high CO values occur over the southern Indian ocean, southern Australia and New Zealand, the North Atlantic, and the far northern and southern reaches of the Pacific ocean. Just as striking as these areas of high CO values are the vast areas of very low CO that occur over the central Pacific and in a band stretching from Central America across the Atlantic, over the Sahara, and into western Asia. Some these features are readily explained by correlation with major source areas of CO emissions. For example, the maxima which occur over southern Africa and central South America have been linked to biomass burning activities (Watson *et al.*, 1990 and Connors *et al.*, 1991). However, other features, such as the high values over the southern Indian ocean and over the northeastern portion of Asia, are not as easily linked to known areas of large CO emissions. Also puzzling is the lack of a well-defined plume associated with North America, which is known to be a significant source of anthropogenic CO.

MODEL DESCRIPTION

The Global atmospheric Chemistry Model (GChM) is an Eulerian, three-dimensional model that simulates the emission, transport, chemical transformation and surface interactions of tropospheric trace species. It has been used previously to investigate the impact of fair weather cloud venting processes on the long-range transport of CO and CH_4 (Luecken *et al.*, 1989) and to estimate the long-range transport of sulfur from North America and Europe to the North Atlantic (Luecken *et al.*, 1991).

Governing Equation

The mass conservation equation for a gas-phase atmospheric species as simulated by GChM is given by

$$\frac{\partial r_i}{\partial t} + \frac{u}{a\cos\theta}\frac{\partial r_i}{\partial \phi} + \frac{v}{a}\frac{\partial r_i}{\partial \theta} + w_\sigma \frac{\partial r_i}{\partial \sigma} =$$

$$\frac{1}{p_s a^2 \cos^2\theta}\frac{\partial}{\partial \phi}\left(p_s K_h \frac{\partial r_i}{\partial \phi}\right) + \frac{1}{p_s a^2 \cos\theta}\frac{\partial}{\partial \theta}\left(p_s \cos\theta\, K_h \frac{\partial r_i}{\partial \theta}\right) + \left(\frac{M_a g}{p_s}\right)^2 \frac{\partial}{\partial \sigma}\left(c^2 K_z \frac{\partial r_i}{\partial \sigma}\right) + R_i + CT_i$$

where ϕ and θ are longitude and latitude respectively, σ is the vertical coordinate expressed in terms of normalized pressure

$$\sigma = p/p_s \ ,$$

p is the pressure at the current vertical level, and p_s is the corresponding pressure at the surface. Further, r_i is the mixing ratio of species i, u and v are the curvilinear velocity components toward east and north, respectively, w_σ is the vertical velocity component in the σ coordinate system, a is the mean radius of the earth, g is the gravitational acceleration, M_a is the molecular weight of air, K_h and K_z are the horizontal and vertical components of the eddy diffusivity tensor, R_i represents chemical production (or loss) of species i, and CT_i is the change of species i per unit time resulting from convective cloud transport. The boundary conditions applied to these equations account for the inflow and outflow of material from the model domain through surface exchange, emission of trace species at the surface, and advection across the model's upper boundary.

Meteorology and Model Transport

Meteorological data from the European Centre for Medium-Range Weather Forecasting (ECMWF) for September 1 through October 15, 1984, were used to drive the GChM simulations reported here. The ECMWF data for this time period are provided on a 1.875° latitude-longitude grid with 16 vertical levels and at 6-h time intervals. The data include horizontal winds, vertical velocity, temperature, humidity, cloud cover, and several surface parameters. The current GChM simulations used the lowest 14 levels (surface to 100 hPa) and a 3.75° horizontal grid resolution.

Advective transport in the model is calculated using a version of the Bott algorithm (Easter, 1993) with 1-h time steps. Vertical turbulent transport is calculated with an implicit in time, centered in space finite difference algorithm. Spatially and temporally varying eddy diffusivity coefficients are calculated according to the procedure of Carmichael (1979). Horizontal turbulent transport is neglected in these simulations.

The parameterization of convective clouds is based on the model of Walcek and Taylor (1986) and is similar to that used in the Regional Acid Deposition Model (Chang *et al.*, 1987). When convective clouds are present over a grid cell, the convective cloud volume (determined by cloud base, cloud top, and areal coverage) is filled with air from below cloud base plus air entrained from the cloud top model level. This takes place over the convective cloud lifetime (assumed 1 h), and then the cloud dissipates. The process of filling the cloud volume transports trace species from below cloud base to higher altitudes. The amount of vertical transport is dependent on the cloud volume and thus the cloud areal coverage (cloud base and cloud top are determined by the temperature and moisture vertical profiles). In the simulations presented here, the areal coverage for convective clouds was taken to be the total cloud coverage from the ECMWF analyses when that coverage was below 35%. As discussed below, convective transport has a major impact on the simulated CO concentrations at upper model levels. We plan to investigate other methods for parameterizing convective transport.

Chemistry

The version of GChM used for this work accounts for the kinetic reactions of CO and CH_4 that occur in the remote troposphere. The gas-phase mechanism of Lelieveld and Crutzen (1990) has been used as the basis for GChM chemical transformations. To reduce the computational burden of the chemical calculations within the model, several simplifying assumptions and techniques have been implemented. First, a latitude-altitude distribution of ozone mixing ratios is specified within the model, based on the climatological distribution of Fishman and Crutzen (1978). Further, NO_x vertical profiles for each grid column are calculated during the simulation based on the implementation of Peters and Jouvanis (1979) and Kitada and Peters (1982). In their formulation, a NO_x vertical profile is specified for each vertical column based on the CO emissions that are specified for that surface grid cell. Since CO emissions in each grid cell are time varying, the NO_x profiles generated by this methodology change dynamically during simulation runtime. Finally, the pseudo-steady-state approximation (PSSA) is imposed at each grid point for all species in the chemistry mechanism except for CO and CH_4. The combination of prescribed NO_x and O_3 distributions and the application of PSSA allows a set of algebraic relationships to be formulated for the calculation of OH radical concentrations. A simple iterative procedure is used to solve the algebraic equations for OH, which is then used to integrate the chemical rate equations of CO and CH_4. To test the accuracy of this simplification procedure, a series of box model chemistry simulations were performed in which the simplified chemical scheme was compared to a full integration of the rate equations with no PSSA applied. The error in CO and CH_4 mixing ratios calculated by the simplified procedure as compared to the full integration was less than 1 percent for most NO_x and O_3 conditions.

CO and CH_4 Emissions

Due to the simplifications made to the chemical transformation calculations, only the emissions of CO and CH_4 were required for the current GChM simulations. Both CO and CH_4 emissions data were taken from the work of DeHaven (1980) and updated based on current knowledge. Table 1 presents a breakdown by category of the emissions used in the current study and a comparison with other investigations.

The major sources of CO are well known, although the exact magnitudes of these sources are uncertain. Emissions from fossil fuel combustion, mainly from automobile exhaust, are the best known and have been estimated by Logan *et al.* (1981) to lie in the range 400-1000 Tg/yr, while Seiler and Conrad (1987) have estimated 440-840 Tg/yr. CO emissions from biomass burning are much less certain and have been estimated at 310-1250 Tg/yr by Logan *et al.* (1981) and at 400-1600 Tg/yr by Seiler and Conrad (1987). The large range in these values reflects uncertainties in both the total amount of biomass consumed and in the amount of CO emitted per kg of biomass combusted. Another significant source of CO is the atmospheric oxidation of anthropogenic and natural nonmethane hydrocarbons. Although the source of CO resulting from the oxidation of anthropogenic hydrocarbons is probably small (Logan *et al.*, 1981), the amount of CO generated from natural hydrocarbons has been variously estimated at 280-1200 Tg/yr by Logan *et al.* (1981), 400-1400 Tg/yr by Seiler and Conrad (1987) and 774 Tg/yr by Warneck (1988). Oxidation of CH_4 represents a further 300-900

Table 1. Carbon Monoxide and Methane Emissions (Tg/yr)

Carbon monoxide	*Logan et al. (1981)*	*Seiler and Conrad (1987)*	*Present study*
Anthropogenic fuel use	500	640	570
Oxidation of hydrocarbons	780	975	878
Biomass burning	605	1000	803
Miscellaneous	40	117	0
TOTAL	1925	2732	2251

Methane	*Fung et al. (1991)*	*Present study*
Enteric fermentation	80	99
Wetlands, rice patties, etc.	255	256
Biomass burning	55	55
Industrial	75	75
Miscellaneous	35	0
TOTAL	500	485

Tg/yr source (Seiler and Conrad, 1987) of atmospheric CO. The total amount of CO generated from these major sources plus several minor ones (direct emission by plants, from the ocean, and from soils) is thought to be on the order of 3000 Tg/yr (Warneck, 1988). CH_4 emissions for the current simulations have been scaled from the work of DeHaven (1980) to correspond approximately to the results of Fung *et al.* (1991).

RESULTS AND DISCUSSION

A total of 14 GChM simulations have been performed with a horizontal resolution of 3.75°. The "base case" simulation was performed using GChM's full representation of chemical and physical processes and our best estimates for emissions. To gauge the sensitivity of the model's output when various model components are perturbed from their base case values, thirteen sensitivity simulations were performed. Results from these sensitivity simulations are presented in Table 2 as changes in the average CO mixing ratio in several model sub-domains over the last 15 days (October 1-15, 1984) of the specified simulation. The sensitivity results of Table 2 indicate that the simulated CO is not greatly sensitive to the assumed NO_x or O_3 distributions, changing no more than 5-10 percent for doubled and halved NO_x and O_3 values. Further, the simulated CO is rather insensitive to the formulation of the boundary layer parameterization. The base case simulation contains a boundary layer eddy diffusivity parameterization that allows for the diurnal growth and collapse of the mixed layer based on local stability and surface characteristics. In the constant mixed layer simulation, the mixed layer depth was fixed at the maximum depth of the base case simulation (1740 m, the top of model layer 5) and had no diurnal variation. As evidenced by the small changes in average CO mixing ratio for this simulation, the lack of a diurnally varying mixed layer had little impact on CO distributions. Likewise, in sensitivity simulations where the maximum mixed layer depth was forced to 1050 m and 2620 m, little change was observed in the average CO mixing ratio.

Two simulations were performed where total CO emissions were increased and decreased by 50 percent. As seen in Table 2, increasing total CO emissions increased the global average CO mixing ratio 27 percent, while halving total emissions decreased the average mixing ratio by 25 percent. In the base simulation, CO production from CH_4 oxidation was equal to 56 percent of the total CO emissions. Thus, increasing (decreasing) the CO emissions by 50 percent changes the overall CO source strength by +32 percent (or -32 percent). Due to the nonlinear effects of chemical feedbacks, the changes in global average CO mixing ratio do not respond linearly to changes in CO emissions. Further, three simulations were performed where each of the major CO emissions categories were omitted. The response of the global average CO mixing ratio resulting from these simulations follows that expected from the relative magnitude of emissions from each category. The largest source category is CO emissions from nonmethane hydrocarbon oxidation; omitting this source reduced the global average mixing ratio by 20 percent. Omitting anthropogenic and biomass burning CO emissions resulted in a global average mixing ratio reduction of 14 percent and 15 percent, respectively.

Figure 1 presents the CO mixing ratio field in the first model layer for the base case simulation, averaged over October 1-15, 1984, corresponding to the time during which the MAPS CO measurements were obtained. The surface CO distribution is heavily dominated by major emission sources. Mixing ratio maxima occur near the major emission sources of eastern North America, Europe, central South America, and central and southern Africa. Peak mixing ratios > 300 ppb occur over eastern North America, central South America and central and southern Africa, while remote regions (e.g., southern Pacific) exhibit mixing ratios < 45 ppb. The model produces a significant hemispheric asymmetry of CO mixing ratios, ranging from 75-150 ppb in the remote northern hemisphere to < 45 ppb in the remote southern hemisphere.

Gas-filter radiometer measurements made during the MAPS experiment correspond to a vertically integrated

Table 2. Summary of GChM Simulations for October 1-15, 1994. For base case run, given values are average CO (ppbv) for indicated model domain. For other simulations, given values are percent changes relative to the base case.

	Model Sub-Domain						
Domain	Global	Global	Global	Cen Africa	E NA	E Europe	NE Siberia
Model Layer	1-14	1	11	11	11	11	11
Simulation							
Base	66.5	87.1	62.4	110.1	79.4	85.8	94.9
CO Emissions x 1.5	26.8	31.8	26.1	39.9	31.5	32.9	34.0
CO Emissions x 0.5	-25.2	-30.6	-24.3	-36.5	-30.1	-31.5	-33.0
Anthropogenic CO Emissions Removed	-13.8	-18.8	-12.0	-1.2	-34.1	-30.9	-31.0
Biomass Burning CO Emissions Removed	-14.6	-17.4	-15.7	-39.8	-6.3	-6.8	-5.4
CO Emissions from NMHC Oxidation Removed	-20.2	-23.4	-19.0	-27.6	-18.1	-23.8	-28.2
NO_x mixing ratios x 0.5	6.3	4.9	7.2	7.8	6.0	5.6	4.3
NO_x mixing ratios x 2.0	-6.4	-5.0	-7.4	-7.2	-6.0	-5.6	-4.4
O_3 mixing ratios x 0.5	4.2	3.4	4.7	5.8	3.9	3.6	2.3
O_3 mixing ratios x 2.0	-5.0	-4.1	-5.6	-6.6	-4.8	-4.5	-3.4
Constant mixed layer depth=1740m	0.2	-2.6	-0.2	0.5	-0.8	-1.0	-1.7
Maximum mixed layer depth=2620m	-0.1	-2.7	0.5	0.2	0.9	1.4	2.0
Maximum mixed layer depth=1050m	0.4	3.9	0.0	0.4	-0.3	-0.4	-0.9
No convective cloud transport	-3.7	19.3	-26.7	-62.1	-35.3	-27.3	-15.8

Sub-Domain	Description	Longitude Range	Latitude Range
Cen Africa	Central Africa	13°E to 36°E	21°S to 9°N
E NA	Eastern North America	92°W to 69°W	32°N to 51°N
E Europe	Eastern Europe	2°E to 43°E	43°N to 69°N
NE Siberia	Northeastern Siberia	84°E to 126°E	54°N to 77°N

CO mixing ratio where the strength of the radiometer signal is a function of altitude. Since the peak signal from the CO instrument occurs at an altitude corresponding to level 11 (~350 hPa) in the model domain, the CO mixing ratio distribution in the mid-troposphere at model level 11 is presented in Figure 2 for the base case simulation, averaged over October 1-15. Accounting for the systematic 20-40 percent low bias in the MAPS data, the distribution of CO produced by the model compares favorably with the MAPS data during this time period. Major features of the distribution that are common with the satellite data include: (i) peak CO mixing ratios occur over central South America and central and southern Africa; (ii) an extensive area of elevated CO occurs over northern Asia; (iii) no well-defined plume of elevated CO from North America is apparent; and, (iv) the lowest mixing ratios occur over the southern Pacific and the far southern Atlantic while decreased CO values occur in a band extending from Central America, over northern Africa, and over southern Asia.

Although the model result and the MAPS satellite data agree very well, there are some discrepancies. For example, the location of the maxima over central South America and Africa occur farther southward in the satellite data than in the model results, indicating either greater horizontal transport or a spatial difference between the model's assumed emission sources and the actual location of biomass fires during October 1984. Further, the MAPS data show indications of a CO plume extending from southern Africa across the far southern Indian ocean and possibly swinging northward across New Zealand and southern Australia. The model distribution also exhibits a plume originating in Africa and extending across the Indian ocean; however, the model-produced plume occurs farther north and contains 10-20 ppb lower CO values than does the satellite data. Lastly, a band of lower CO values extending from northern Africa across eastern Europe and into central Asia is

Figure 1. CO mixing ratio distribution from GChM model level 1 (~1010 hPa) averaged over October 1-15, 1984 for the base case simulation.

Figure 2. CO mixing ratio distribution at GChM model level 11 (~350 hPa) averaged over October 1-15, 1984 for the base case simulation. Model level 11 corresponds to the altitude of maximum signal strength from the MAPS gas-filter radiometer.

clearly indicated in the MAPS data; the model result does exhibit lower mixing ratios in this region as compared to the areas of peak values, however, the CO values range from 55-75 ppb as compared to < 60 ppb observed in the MAPS experiment.

Figure 3 presents the model produced CO mixing ratio distribution at model level 11 for the sensitivity simulation where the convective cloud transport parameterization was disabled within the model. The results of Figure 3 are presented with the same shading contours as Figure 2 for ease of comparison. As is readily observed, convective cloud transport plays a significant role in the amount of CO that is transported to model layer 11, implying that the CO distribution as observed during the MAPS experiment is largely the product of surface emissions vented rapidly to the mid-troposphere by convective activity associated with clouds. These results support the conclusions of Newell *et al.* (1988), Connors *et al.* (1989), Watson *et al.* (1990), and

Figure 3. CO mixing ratio distribution at GChM model level 11 (~350 hPa) averaged over October 1-15, 1984 for the no cloud convection simulation. Model level 11 corresponds to the altitude of maximum signal strength from the MAPS gas-filter radiometer.

Connors *et al.* (1991), that cloud convective activity serves to transport boundary layer CO into the free troposphere where it can be transported long distances away from its point of emission. As documented in Table 2, the average CO mixing ratio in model layer 11 is 27 percent lower without the convective cloud parameterization enabled. Likewise, CO mixing ratios in the lowest model layer are 19 percent greater, indicating that in the base case simulation a substantial amount of material within the boundary layer is transported to higher model levels. In the central African sub-domain, a decrease of 62 percent in the domain-averaged CO mixing ratio occurred when the convective cloud parameterization was disabled, implying that a majority of the CO observed over this region in the MAPS data is brought to this level by cloud convective activity.

CONCLUSION

The GChM atmospheric chemistry and transport model has been used to analyze the mid-tropospheric CO dataset obtained from NASA's Measurement of Air Pollution by Satellites (MAPS) program. Fourteen simulations with a 3.75° horizontal resolution have been performed, including a base case and 13 sensitivity runs. The model reproduces many, but not all, of the major features of the MAPS dataset. Locations of peak CO mixing ratios associated with biomass burning as observed in the MAPS experiment are slightly farther south than the model result, indicating either greater horizontal transport than present in the model representation or a spatial difference between the location of modeled biomass fires and actual fires. The current version of GChM was shown to be relatively insensitive to the magnitude of the prescribed NO_x and O_3 global distributions and very insensitive to the depth of the mixed layer as parameterized in the model. Cloud convective transport was shown to play an important role in venting boundary layer CO to the free troposphere. This result agrees with prior meteorological analyses of the MAPS dataset (Newell *et al.*, 1988; Connors *et al.*, 1989; Watson *et al.*, 1990; and Connors *et al.*, 1991) that have indirectly inferred the presence of convective activity through satellite-based information. Work is continuing to analyze the results of these simulations further and to perform more detailed comparisons between model results and MAPS data.

Acknowledgement

This research was funded through the Laboratory Directed Research and Development program of Pacific Northwest Laboratory. Pacific Northwest Laboratory is operated for the U. S. Department of Energy by Battelle Memorial Institute under Contract DE-AC06-76RLO 1830.

REFERENCES

Carmichael, G. R.,1979, Development of a regional transport/transformation/removal model for SO_2 and sulfate in the eastern United States, Ph.D. dissertation, University of Kentucky, Lexington, Kentucky.

Chang, J. S., R. A. Brost, I. S. A. Isaksen, S. Madronich, P. Middleton, W. R. Stockwell, and C. J. Walcek, 1987, A three-dimensional Eulerian acid deposition model: Physical concepts and formulation, *J. Geophys. Res.*, 92:14681-14700.

Connors, V. S., Cahoon, D. R., Reichle, H. G., Brunke, E.-G., Garstang, M., Seiler, W., and Scheel, H. E., 1991, Savanna burning and convective mixing in southern Africa: Implications for CO emissions and transport, in "Global Biomass Burning: Atmospheric, Climatic, and Biospheric Implications", J. S. Levine, ed., MIT Press, Cambridge, Massachusetts, 147-159.

Connors, V. S., Miles, T., and Reichle, H. G., 1989, Large-scale transport of a CO-enhanced air mass from Europe to the Middle East, *J. Atmos. Chem.*, 9:479-496.

Crutzen, P. and Zimmerman, P.,1991, The changing chemistry of the troposphere, *Tellus*, 43AB:136-151.

DeHaven, D. A., 1980, CO and CH_4 sources and their effects on the CO-CH_4 budgets, M.S. Thesis, University of Kentucky, Lexington, Kentucky.

Easter, R. C., 1993, Two modified versions of Bott's positive-definite numerical advection scheme, *Mon. Wea. Rev.*, 121:297-304.

Fishman, J., and Crutzen, P. J., 1978, The origin of ozone in the troposphere, *Nature*, 274:855-858.

Fung, I., John, J., Lerner, J., Matthews, E., Prather, M., Steele, L., and Fraser, P., 1991, Three-dimensional model synthesis of the global methane cycle, J. Geophys. Res., 96:13033-13065.

Kitada, T. and Peters, L. K., 1982, A three-dimensional transport-chemistry analysis of CO and CH_4 in the troposphere, in "AMS Second Symposium on the Composition of the Nonurban Troposphere", Williamsburg, Virginia, 96-101.

Kwok, H. C. W., Langlois, W. E., and Ellefsen, R. A., 1971, Digital simulation of the global transport of carbon monoxide, *IBM J. Res. Develop.*, 15:3-9.

Lelieveld, J., and Crutzen, P.J., 1990, Influence of cloud photochemical processes on tropospheric ozone, *Nature*, 343:227-233.

Logan, J. A., Prather, M. J., Wofsy, S. C., McElroy, M. B., 1981, Tropospheric chemistry: A global perspective, *J. Geophys. Res.*, 86:7210-7254.

Luecken, D. J., Berkowitz, C. M., Bader, D. C., Vukovich, F. M., and Glatzmeir, G. C., 1989, The role of fair weather cumulus clouds in the long range transport of carbon monoxide and methane, American Geophysical Union Spring Meeting, Baltimore, Maryland.

Luecken, D. J., Berkowitz, C. M., and Easter, R. C., 1991, Use of a three-dimensional cloud-chemistry model to study the transatlantic transport of soluble sulfur species, *J. Geophys. Res.*, 96:22477-22490.

Newell, R. S., Connors, V. S., Reichle, H. G., 1988, Regional studies of potential CO sources based on space shuttle and aircraft measurements, *J. Atmos. Chem.*, 6:61-81.

Peters, L. K., and Jouvanis, A. A., 1979, Numerical simulation of the transport and chemistry of CH_4 and CO in the troposphere, *Atmos. Environ.*, 13:1443-1462.

Pinto, J. P., Yung, Y. L., Rind, D., Russell, G. L., Lerner, J. A., Hansen, J. E., and Hameed, S., 1983, A general circulation model study of atmospheric carbon monoxide, *J. Geophys. Res.*, 88:3691-3702.

Reichle, H. G., Connors, V. S., Holland, J. A., Hypes, W. D., Wallio, H. A., Casas, J. C., Gormsen, B.B., Saylor, M. S., and Hesketh, W. D., 1986, Middle and upper tropospheric carbon monoxide mixing ratios as measured by a satellite-borne remote sensor during November 1981, *J. Geophys. Res.*, 91:10865-10887.

Reichle, H. G., Connors, V. S., Holland, J. A., Sherrill, R. T., Wallio, H. A., Casas, J. C., Condon, E.P., Gormsen, B. B., and Seiler, W., 1990, The distribution of middle tropospheric carbon monoxide during early October 1984, *J. Geophys. Res.*, 95:9845-9856.

Saylor, R. D., and Peters, L. K., 1990, The contribution of anthropogenic emissions to the global distribution of CO in the troposphere, Symposium on the Chemistry of the Global Atmosphere, Commission on Atmospheric Chemistry and Global Pollution, Chamrousse, France.

Saylor, R. D., and Peters, L. K., 1991, The global numerical simulation of the distribution of CO in the troposphere, "Air Pollution Modeling and Its Application VIII", H. van Dop and D. G. Steyn, eds., Plenum Press, New York, 485-496.

Seiler, W., and Conrad, R., 1987, Contribution of tropical ecosystems to the global budget of trace gases, especially CH_4, H_2, CO and N_2O, in "The Geophysiology of Amazonia", R.E. Dickinson, ed., John Wiley & Sons, New York.

Seinfeld, J., 1986, "Atmospheric Chemistry and Physics of Air Pollution", John Wiley & Sons, New York.

Walcek, C. J., and G. R. Taylor, 1986, A theoretical method for computing vertical distributions of acidity and sulfate production within cumulus clouds, *J. Atmos. Sci.*,43:339-355.

Warneck, P., 1988, "Chemistry of the Natural Atmosphere", Academic Press, New York.

Watson, C. E., Fishman, J., and Reichle, H. G., 1990, The significance of biomass burning as a source of carbon monoxide and ozone in the southern hemisphere tropics: A satellite analysis, *J. Geophys. Res.*, 95:16443-16450.

Figure 1

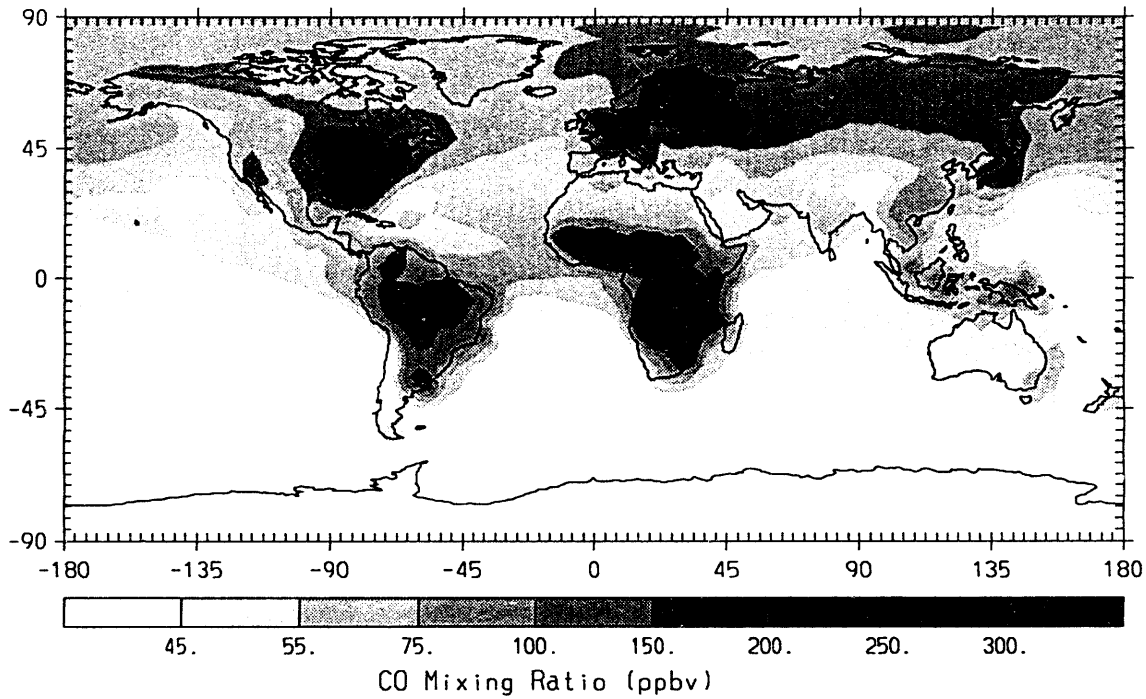
90
45
0
-45
-90
-180
-135
-90
-45
0
45
90
135
180
45.
55.
75.
100.
150.
200.
250.
300.
CO Mixing Ratio (ppbv)

Figure 2

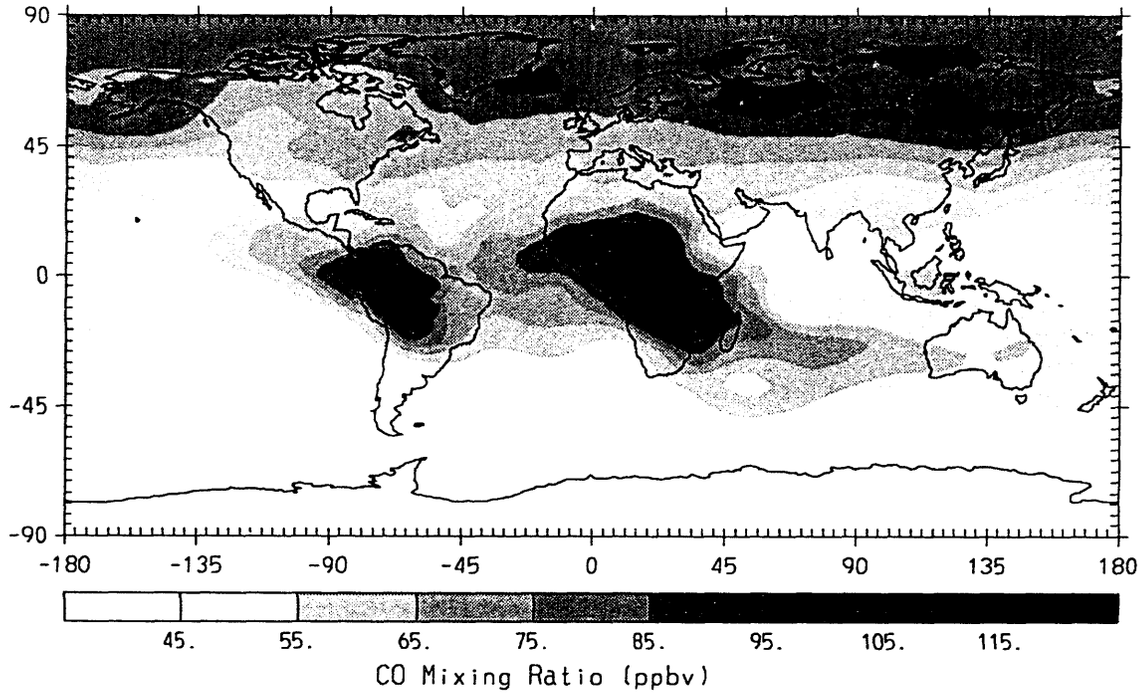
90
45
0
-45
-90
-180
-135
-90
-45
0
45
90
135
180
45.
55.
65.
75.
85.
95.
105.
115.
CO Mixing Ratio (ppbv)

Figure 3

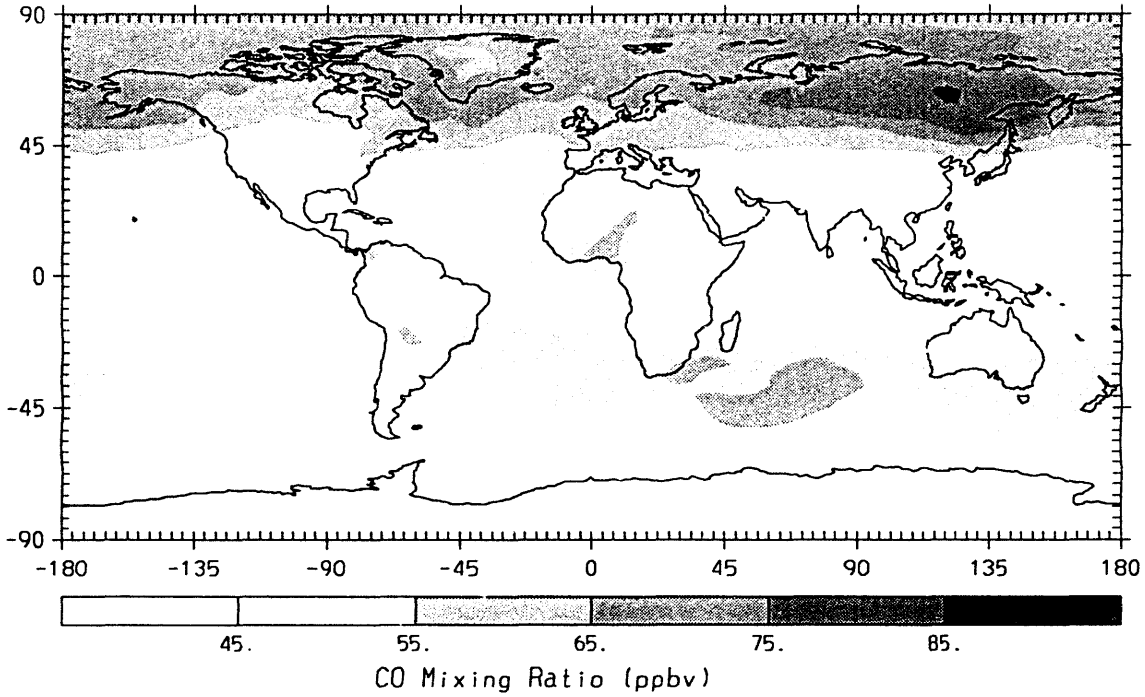
90
45
0
-45
-90
-180
-135
-90
-45
0
45
90
135
180
45.
55.
65.
75.
85.
CO Mixing Ratio (ppbv)

DATE
FILMED
5/20/94

END